Journal of Molecular Catalysis A: Chemical 301 (2009) 152–158

Contents lists available at ScienceDirect

Journal of Molecular Catalysis A: Chemical

journal homepage: www.elsevier.com/locate/molcata

# Ethane dehydrogenation over pore-expanded mesoporous silica supported chromium oxide: 1. Catalysts preparation and characterization

T.V. Malleswara Rao, Yong Yang, Abdelhamid Sayari*

*Department of Chemistry, University of Ottawa, Ottawa, ON, K1N 6N5, Canada*

ARTICLE INFO

*Article history:*
Received 5 September 2008
Received in revised form
27 November 2008
Accepted 27 December 2008
Available online 9 January 2009

*Keywords:*
Ethane dehydrogenation
Chromium oxide
MCM-41
Pore-expanded MCM-41
XPS

ABSTRACT

Pore-expanded MCM-41 silica was prepared in two steps, namely synthesis of MCM-41 in the presence of cetyltrimethylammonium bromide (CTAB) at 100 °C followed by a hydrothermal pore expansion treatment in the presence of dimethyldecylamine (DMDA) at 120 °C for 72 h. The as-synthesized material (PE-MCM-41), the material obtained after selective ethanol extraction of DMDA (PE-MCM-41E) and the organic-free material obtained after calcination of PE-MCM-41 (PE-MCM-41C) were used as supports for chromium oxide up to a chromium loading of 7 wt.%. All catalysts were thoroughly characterized by X-ray diffraction, $N_2$ adsorption, temperature programmed reduction (TPR), Raman and X-ray photoelectron spectroscopy (XPS), and used for ethane dehydrogenation (DH). $N_2$ adsorption measurements showed that the pore and surface characteristics strongly depend on the catalyst preparation method and relatively independent of chromia loading. The structural properties of the chromium-loaded materials were associated with the effect of water on the support, which is dependent on how well the silica framework is protected by the occluded surfactant(s) against direct contact with water. XPS analysis showed that in most cases, the surface chromium contained significant amounts of Cr(III) and Cr(VI) and minor amounts of Cr(II). Furthermore, $H_2$-TPR results revealed that the extent of reduction of the catalysts depend on the chromia loading and the preparation method.



## 1. Introduction

Catalytic ethane dehydrogenation (DH) is an important reaction for the production of high demand ethylene [1–3]. Supported chromium oxide catalysts were found to be effective for DH of ethane [4–9]. However, the nature of active surface chromium species is still being debated as both Cr(II) [4,5] and Cr(III) [9–12] species were reported to be the active sites for light alkane DH. Recent work showed that MCM-41 is an attractive support for chromia-based catalysts, which are employed in many catalytic reactions including oxidative dehydrogenation, dehydrogenation in the presence of $CO_2$ and ethylene polymerization [13–16]. The current contribution deals with the preparation and characterization of pore-expanded supported chromium oxide catalysts for ethane DH. Investigation of their catalytic properties and the nature of active sites in ethane DH will be reported in a companion paper [17].

Recent studies by Sayari and co-workers [18–20] showed that due to its unique properties such as high surface area (>1000 $m^2/g$), adjustable pore size (up to 25 nm) and high pore volume (up to 3.6 $cm^3/g$), pore-expanded mesoporous silica finds many applications in adsorption [21–23] and catalysis [24]. Thus, the present study extends the application of pore-expanded mesoporous silica as support for stable and highly selective chromium oxide catalysts for DH of ethane.

## 2. Experimental

### 2.1. Materials

Cab-O-Sil M-5 fumed silica from Cabot was used as the silica source for the preparation of pore-expanded mesoporous silica. Cetyltrimethylammonium bromide (CTAB, Aldrich) and tetramethyl ammonium hydroxide (TMAOH 25%, balance water, Aldrich) were used as structure directing agent and for pH adjustment, respectively. The post-synthesis pore expander agent was dimethyldecylamine (DMDA 97% purity, Aldrich). Chromium nitrate nonahydrate ($Cr(NO)_3{\cdot}9H_2O$, Aldrich) was used as precursor for supported and unsupported chromium oxide.

### 2.2. Catalysts synthesis

As shown schematically in Fig. 1, pore-expanded MCM-41 silica was prepared in two stages based on a procedure described elsewhere [18–20]. An amount of 578.6 g of TMAOH 25% was

* Corresponding author. Tel.: +1 613 562 5483; fax: +1 613 562 5170.
*E-mail address:* abdel.sayari@uottawa.ca (A. Sayari).

1381-1169/$ – see front matter © 2009 Elsevier B.V. All rights reserved.
doi:10.1016/j.molcata.2008.12.026

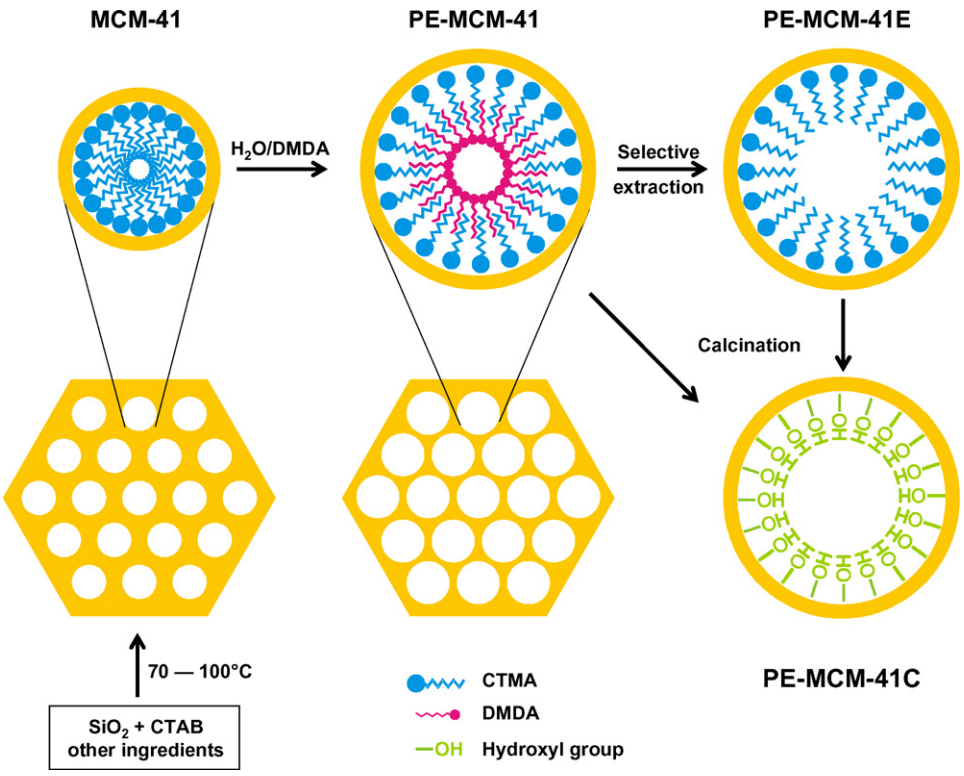


**Fig. 1.** Schematic representation of pore expansion of mesoporous MCM-41 silica.

diluted in 5500 g of water under vigorous stirring in an 8 L stainless steel vessel. Afterwards, CTAB (820 g) was added, and stirred for 15 min. Subsequently, 328.4 g of Cab-O-Sil fumed silica was added. After mixing for 30 more minutes at ambient temperature, the resulting gel was placed in an oven and stirred at 100 °C under autogenous pressure for 40 h. The obtained material was filtered, thoroughly washed with water and dried at ambient conditions. The obtained material whose pores were filled with surfactant will be designated *as-synthesized* MCM-41. The *as-synthesized* MCM-41 underwent a hydrothermal pore expansion treatment using DMDA as expander agent. An emulsion was prepared by adding 437.5 g of DMDA in 5250 g of water under vigorous stirring at ambient temperature. Subsequently, 350 g of as-synthesized MCM-41 was added and the mixture was kept under stirring for 15 more minutes. The resulting suspension was heated in a stainless steel closed vessel at 120 °C under continuous stirring for 72 h. The material was then filtered, washed with water, and dried in ambient air. This material will be designated as PE-MCM-41. Selective removal of DMDA in the presence of ethanol afforded PE-MCM-41E, whereas calcination of PE-MCM-41 in air at 700 °C for 6 h to remove both the expander agent and the template gave rise to PE-MCM-41C.

To investigate the effect of the preparation method on the performance of supported chromium oxide catalysts in ethane DH reaction, chromium oxide was supported on pore-expanded MCM-41 silica in three different ways as described below.

### 2.2.1. Method I

The as-synthesized PE-MCM-41 silica was added to a solution containing predetermined amounts of precursor ($Cr(NO)_3{\cdot}9H_2O$) under stirring conditions in order to prepare catalysts with different loadings. The mixture was filtered, washed with distilled water and dried overnight in air at 45 °C. The obtained solid was heated in flowing $N_2$ to 700 °C, then calcined in flowing air at 700 °C for 6 h to form the supported chromium oxide catalysts. The obtained catalysts will be denoted as *x*Cr/PE-MCM-41, where *x* is the wt.% loading corresponding to $Cr_2O_3$. Samples with chromia loading higher than ~5 wt.% were prepared by Method II described below.

### 2.2.2. Method II

Supported chromium oxide catalysts were prepared by the incipient wetness impregnation technique using PE-MCM-41E as support. Incipient volume of solution containing a predetermined amount of chromium nitrate and the PE-MCM-41E support were intimately mixed and the mixture was kept in a dessiccator overnight followed by heating in flowing $N_2$ up to 700 °C. Finally the samples were calcined in air at 700 °C for 6 h. The catalysts thus obtained will be designated as *x*Cr/PE-MCM-41E, where *x* is the wt.% loading corresponding to $Cr_2O_3$.

### 2.2.3. Method III

PE-MCM-41C was used as support for the deposition of chromium oxide by the incipient wetness impregnation technique as described in Section 2.2.2. The only difference between Methods II and III lies in the nature of the impregnated support. A sample with ~5 wt.% chromia loading was prepared using this method and referred to as 5Cr/PE-MCM-41C.

To obtain comparable chromia loadings using the above three methods, one should take into account the amounts of expander (DMDA) and surfactant template (CTMA) present in PE-MCM-41 and PE-MCM-41E. Separate experiments employing selective extraction of DMDA by ethanol and calcination of PE-MCM-41 led us to determine the approximate composition as DMDA:CTMA:$SiO_2$ = 45%:26%:29%. Nonetheless, the final chromia loadings were determined by inductively coupled plasma (ICP) measurements using a Varian vista-PRO ICP-mass spectrometer and are presented in Table 1. Bulk $Cr_2O_3$ prepared by thermal decomposition of $Cr(NO)_3{\cdot}9H_2O$ in air at 700 °C for 6 h was also considered for comparison purpose.

**Table 1**
Structural properties of the materials and reduction characteristics of chromium oxide-containing catalysts.

| Sample | wt.%. $Cr_2O_3$ from ICP | BET surface area ($m^2$/g) | Pore volume ($cm^3$/g) | Pore size (nm) | $T_{max}$ values[c] (°C) | $H_2$ consumed ($\times 10^4$ gmol/g cat) | H/Cr[d] |
|---|---|---|---|---|---|---|---|
| PE-MCM-41 | – | 65 | 0.18 (0.62)[a] | – | – | – | – |
| PE-MCM-41E | – | 544 | 1.20 (2.28)[a] | 8.1 | – | – | – |
| PE-MCM-41C | – | 1120 | 2.43 (2.43)[a] | ca. 9.2 | – | – | – |
| 2Cr/PE-MCM-41 | 1.8 | 1102 | 2.25 | 8.4 | 415 | 2.15 | 1.92 |
| 5Cr/PE-MCM-41 | 4.6 | 1065 | 2.14 | 8.4 | 410 | 2.96 | 1.00 |
| 2Cr/PE-MCM-41E | 1.9 | 968 | 1.17 | bmd[b] | 413 | 2.24 | 1.80 |
| 5Cr/PE-MCM-41E | 4.8 | 925 | 1.01 | bmd[b] | 410 | 4.01 | 1.27 |
| 7Cr/PE-MCM-41E | 6.5 | 896 | 0.99 | bmd[b] | 405 | 3.95 | 0.83 |
| 5Cr/PE-MCM-41C | 4.9 | 500 | 0.35 | – | 404 | 6.85 | 2.12 |
| Bulk $Cr_2O_3$ | – | 9 | – | – | 244, 518 | 1.60 | 0.02[e] |

[a] Pore volume per gram of silica (instead of gram of material).
[b] bmd: bimodal pore size distribution.
[c] Maximum reduction temperature.
[d] Based on actual Cr content.
[e] Assuming 100% Cr content.

### 2.3. Catalysts characterization

#### 2.3.1. Pore size distribution and BET surface area measurements

The prepared catalysts and the supports were characterized by $N_2$ adsorption measurements at 77 K using a Micromeritics ASAP 2020 adsorption analyzer. Prior to the measurements, PE-MCM-41 and PE-MCM-41E samples were degassed under vacuum ($1 \times 10^{-5}$ Torr) for 5 h at ambient temperature to avoid thermal decomposition of the organic content of the samples. The PE-MCM-41C and the calcined catalysts were degassed at 250 °C for 5 h. The BET specific surface areas were determined from the adsorption data in the relative pressure ($P/P_0$) range from 0.06 to 0.2. The pore size distributions (PSDs) were calculated from the nitrogen adsorption branch using the Barrett–Joyner–Halenda (BJH) method with Kruk–Jaroniec–Sayari (KJS) correction [25] and the maximum of the PSD was considered as the average pore size. The pore volume was considered as the volume of liquid nitrogen adsorbed at $P/P_0$ = ca. 1.

#### 2.3.2. X-ray diffraction (XRD)

Powder XRD patterns of the samples were acquired with a Philips PW3710 diffractometer using Cu Kα radiation (λ = 1.5418 Å) at 45 kV and 40 mA.

#### 2.3.3. Raman spectroscopy

Raman spectra of materials were collected under ambient conditions with a HORIBA Jobin Yvon LabRam-IR HR800 system equipped with a confocal microscope (Olympus BX-30), notch filter and a 900 grooves/mm gratings [26]. The powdered samples were irradiated with an Ar-ion laser light (λ 514.5 nm), and the backscattered radiation was collected through a 100× objective lens with a 0.9 numerical aperture and detected by a CCD camera. The spectra were acquired in the 400–1200 $cm^{-1}$ range.

#### 2.3.4. Temperature programmed reduction using hydrogen ($H_2$-TPR)

The $H_2$-TPR measurements were performed on an Altamira Instruments temperature programmed system (AMI-200). A sample weight of ca. 0.15 g was loaded in a U-shaped quartz reactor and pretreated in flowing Ar (30 mL/min) at 350 °C for 1 h. After cooling the sample to 40 °C, a 10% $H_2$/Ar mixture flowing at 30 mL/min was introduced into the reactor for TPR measurements. The catalyst sample was heated to a final temperature of 700 °C at a ramping rate of 10 °C/min. The hydrogen consumption was measured by a thermal conductivity detector. Hydrogen pulse calibration was also performed after each TPR experiment for the quantification of TPR data.

#### 2.3.5. X-ray photoelectron spectroscopy (XPS)

XPS measurements of the supported chromium oxide catalysts were performed on a Kratos Axis Ultra DLD (delay-line detector) spectrometer using a focused monochromatized Al Kα radiation (1486.6 eV). The sample was adhered to a double-sided tape on a sample holder and introduced into the treatment chamber. The sample was maintained under high vacuum (~$10^{-8}$ Torr) prior to transferring it to the main XPS analysis chamber, which was maintained at ~$10^{-9}$ Torr. Charging effects of the sample were minimized by employing a low energy electron gun. XPS survey scan spectra were collected using 160 eV analyzer electron pass energy in ~2 min, while the high resolution XPS region scan spectra were obtained at 20 eV pass energy within a short period of time (~12 min) in order to avoid or minimize the photo-reduction of surface chromium species induced by X-rays [27–29]. The binding energies were calibrated using the peak of adventitious carbon (C 1s) at 284.6 eV [29]. Quantitative calculations of the surface atomic concentrations of different elements present in the samples and the composition of different chemical states of surface chromium were obtained by peak fitting of XPS spectra using Vision 2.0 processing software, provided by Kratos Analytical Ltd., UK.

## 3. Results and discussion

### 3.1. Pore size distribution and BET surface area measurements

The $N_2$ adsorption–desorption isotherms for as-synthesized, extracted and calcined pore-expanded mesoporous silica samples and supported chromium oxide catalysts are presented in Figs. 2–4. The PSDs are shown in the inset of the corresponding nitrogen adsorption figures. The isotherms for the PE-MCM-41 and PE-MCM-41E-derived catalysts revealed a hysteresis loop with sharp $N_2$ evaporation and condensation steps indicative of the occurrence of narrow PSDs. Nitrogen hysteresis loops were found to occur for mesoporous materials with pores larger than 4 nm [30,31]. As shown in Fig. 2, nitrogen adsorption isotherms for PE-MCM-41C and all calcined chromium oxide catalysts supported on PE-MCM-41 (prepared by Method I) were of similar shape. The BET surface area, pore volume and average pore sizes of different samples are listed in Table 1. Table 1 and Fig. 2 (inset) show that the samples prepared by Method I exhibit a relatively narrow PSD with the similar pore sizes (8.4 nm vs. 9.2 nm) and slightly lower pore volumes (~2.14–2.25 $cm^3$/g) as compared to PE-MCM-41C (2.43 $cm^3$/g), indicating that chromium deposition by this method did not affect

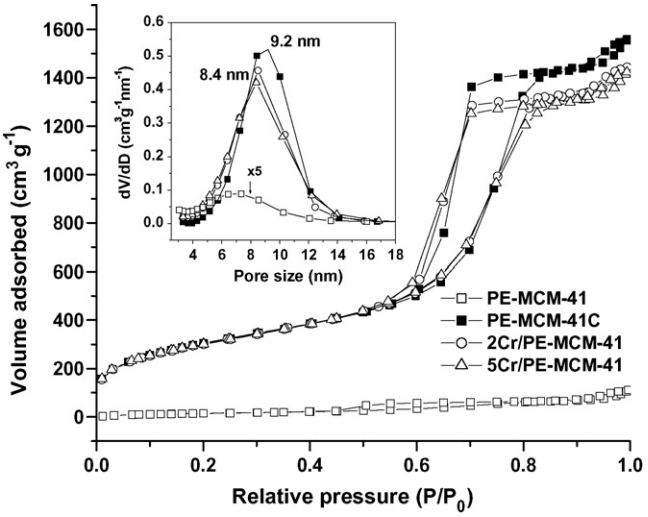


**Fig. 2.** $N_2$ adsorption–desorption isotherms for *x*Cr/PE-MCM-41 catalysts and their PSDs (inset).

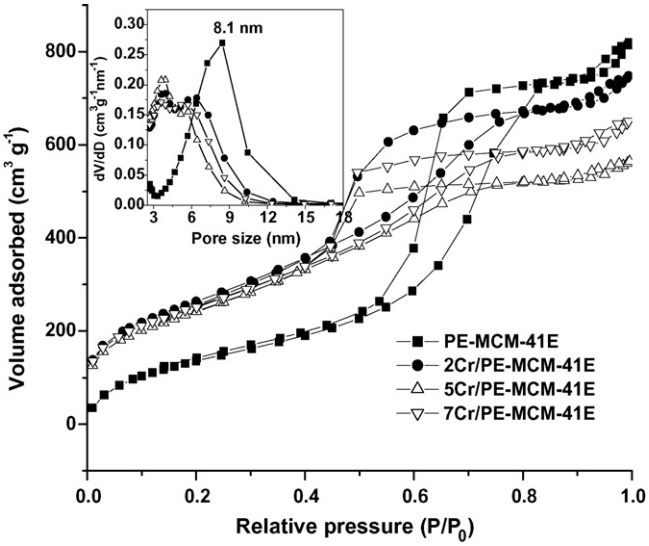


**Fig. 3.** $N_2$ adsorption–desorption isotherms for *x*Cr/PE-MCM-41E catalysts and their PSDs (inset).

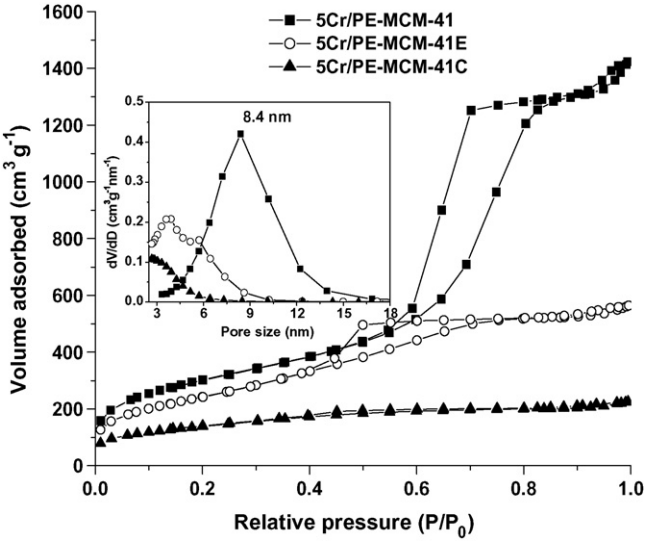


**Fig. 4.** Effect of the preparation method on $N_2$ adsorption–desorption isotherms and PSDs (inset) for the supported chromium oxide catalysts.

the pore structure. Furthermore, the surface areas were also relatively independent of chromia loading on PE-MCM-41.

As shown in Fig. 3, the samples prepared by Method II, i.e., chromium deposition on PE-MCM-41E and further calcination, exhibited a narrow hysteresis loop and a bimodal pore size distribution with maxima at 3.7 and 5.8 nm (see Fig. 2 inset), while the calcined PE-MCM-41E sample had a well defined PSD with an average pore size of 8.1 nm. Notice that air calcination of PE-MCM-41E affords a material with comparable structural properties as PE-MCM-41C. This suggests that chromia deposition by Method II gives rise to partial collapse of the pore structure. For *x*Cr/PE-MCM-41E (*x* = 2–7) samples, the surface areas were relatively independent of chromia loading but slightly lower than that for PE-MCM-41C sample.

In order to compare the effect of all three preparation methods on the structural properties of the catalysts, the isotherms and PSDs of ~5 wt.% chromia-loaded samples are presented in Fig. 4. It is clear from Fig. 4 and Table 1 that the preparation method strongly affects the pore structure of the calcined samples. In particular, chromia deposition on PE-MCM-41C (Method III) resulted in a drastic decrease in surface area with significant decrease in the pore volume of the calcined sample compared to that of PE-MCM-41C, indicating an extensive collapse of the pore structure. Furthermore, in addition to its much smaller pore volume compared to the other types of materials, the 5Cr/PE-MCM-41C sample possessed an ill-defined PSD. The surface areas and pore volumes of the 5Cr series samples prepared by different methods follow the order: 5Cr/PE-MCM-41 (Method I) > 5Cr/PE-MCM-41E (Method II) ≫ 5Cr/PE-MCM-41C (Method III). In addition to the above observations, Figs. 2–4 also show a small hysteresis loop above a relative pressure of 0.9 for all the samples studied, which indicates the occurrence of a small amount of large secondary mesopores in the samples [32]. Thus, the supported chromium oxide (*x*Cr/PE-MCM-41) catalysts prepared by Method I exhibit the highest surface areas (~1100 $m^2$/g), pore sizes (8.4 nm) and pore volumes (>2.1 $cm^3$/g).

To understand why the structural properties of chromium oxide-containing materials deteriorate as the support is freed from its organic content, it is suggested that water is the actual culprit. To substantiate this contention, all three chromium-free pore-expanded mesophases were stirred in water at room temperature for 24 h, separated, dried and calcined. The nitrogen adsorption–desorption isotherms and the PSDs for these materials are shown in Fig. 5. Fig. 5B indicates clearly that PE-MCM-41 was hardly affected by water. However, PE-MCM-41E (Fig. 5C) afforded a material with similar structural properties as *x*Cr/PE-MCM-41E including comparable surface area and pore volume, as well as reduced pore sizes with a bimodal distribution. Finally, the calcined mesophase, PE-MCM-41C, collapsed upon exposure to water leading to an essentially microporous amorphous silica with significantly reduced pore volume (Fig. 5D). The large difference in surface area between water-treated PE-MCM-41C (930 $m^2$/g) and 5Cr/PE-MCM-41C (500 $m^2$/g) may be attributed to the fact that the micropores were blocked by supported chromium oxide.

It is thus inferred that the structural properties of the various chromia-containing catalysts is associated with the effect of water on the support during the materials synthesis. The pore walls of pore-expanded mesoporous silica are quite sensitive to water as they collapse upon direct contact with water, most likely through hydrolysis of siloxane bridges [33]. Indeed, as inferred from its small surface area (<100 $m^2$/g) and pore volume (ca. 0.2 $cm^3$/g), PE-MCM-41 is completely filled with DMDA and CTMA surfactants, and the actual silica pore walls may not come into contact with water when the material is immersed in water. As for PE-MCM-41E, it exhibits a pore volume of ca. 1.2 $cm^3$/g. Since it contains about 50% CTMA, its pore volume based on pure silica would be ca. 2.4 $cm^3$/g, very close to that of PE-MCM-41C. This indicates that the layer of CTA is quite

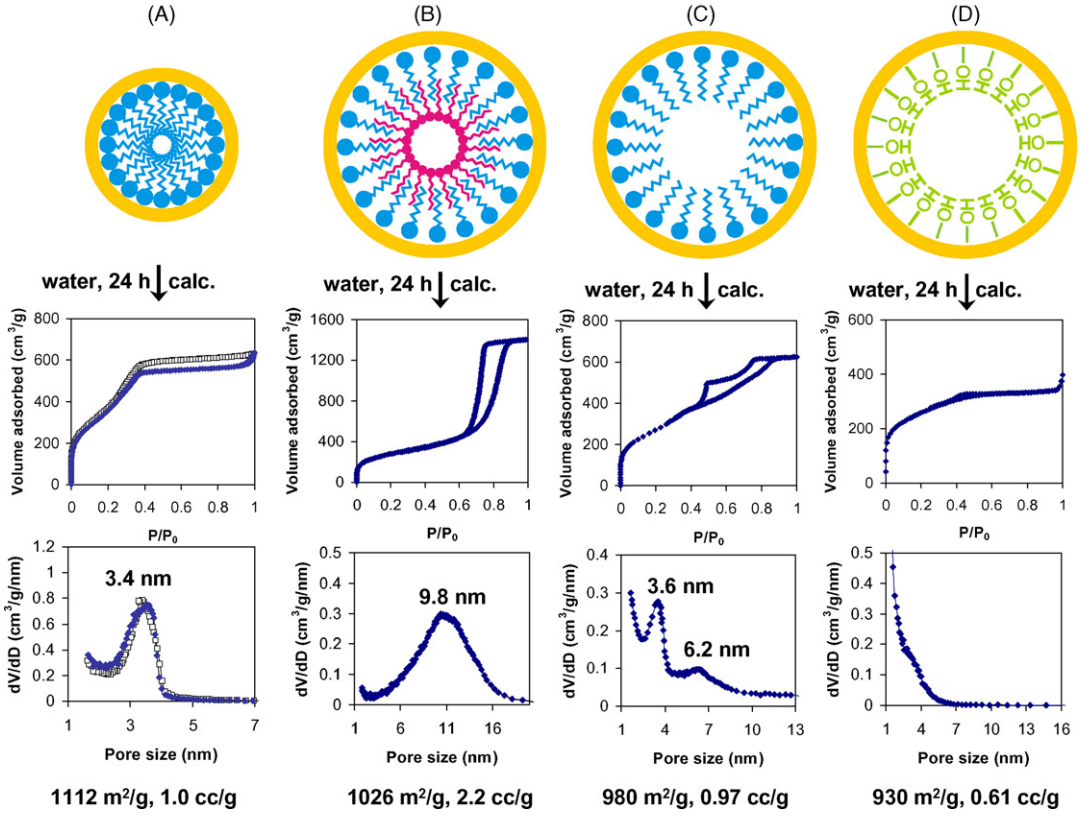


**Fig. 5.** $N_2$ adsorption–desorption isotherms for (A) MCM-41, (B) PE-MCM-41, (C) PE-MCM-41E and (D) PE-MCM-41C samples and the corresponding PSDs after treatment in water followed by air calcination.

porous and does not fully protect the pore walls from direct contact with water, hence the partial collapse of the pore structure during stirring in water, as well as during the incipient wetness impregnation of chromium nitrate. Interestingly, as-synthesized MCM-41 (Fig. 5A) which has much smaller channel size than PE-MCM-41E, but contains similar amount of CTMA surfactant is highly stable in water. This indicates that the amount the CTMA is large enough to protect the pore walls of as-synthesized MCM-41, but not the pore walls of the wider channels PE-MCM-41E.

In summary, to prepare catalysts supported on pore-expanded mesoporous silica while preserving the integrity of the pore structure using a method that involves water such as incipient wetness, impregnation, or precipitation, it is essential to use the as-synthesized PE-MCM-41. Moreover, the role of the occluded organic material is not only to physically protect the silica walls from coming into direct contact with water, but also as shown schematically in Fig. 1, the occurrence of DMDA may create a hydrophilic channel that favors the diffusion of the aqueous phase within the pore channels. Furthermore, being very reactive toward a large number of cations, the amine groups offer a powerful driving force for water-dissolved cations to penetrate deep within the pore structure through direct complexation. Depending on the nature of the cations, upon further reaction such as calcination, reduction, sulfidation, etc., highly dispersed oxides, metals, sulfides, etc. may be prepared. This approach was successfully used for the synthesis of highly dispersed palladium nanoparticles [24] and is being extended to other material formulations.

### 3.2. X-ray diffraction

The powder XRD patterns of PE-MCM-41, PE-MCM-41C and supported chromium oxide samples along with bulk $Cr_2O_3$ are shown in Fig. 6. The PE-MCM-41, PE-MCM-41C and the supported samples showed only a single prominent peak in the low angle region, characteristic of disordered mesoporous silica materials [18]. The samples with low chromia loading (<5%) did not reveal any peaks corresponding to bulk $Cr_2O_3$, suggesting that either the chromium oxide phase is amorphous in nature or the occurrence of $Cr_2O_3$ crystals less than 4 nm in size. However, the ~5 wt.% chromia-loaded samples prepared by all three methods showed peaks corresponding to $Cr_2O_3$. Furthermore, the 5Cr/PE-MCM-41C sample exhibited more intense diffraction peaks compared to 5Cr/PE-MCM-41 and 5Cr/PE-MCM-41E samples, suggesting the

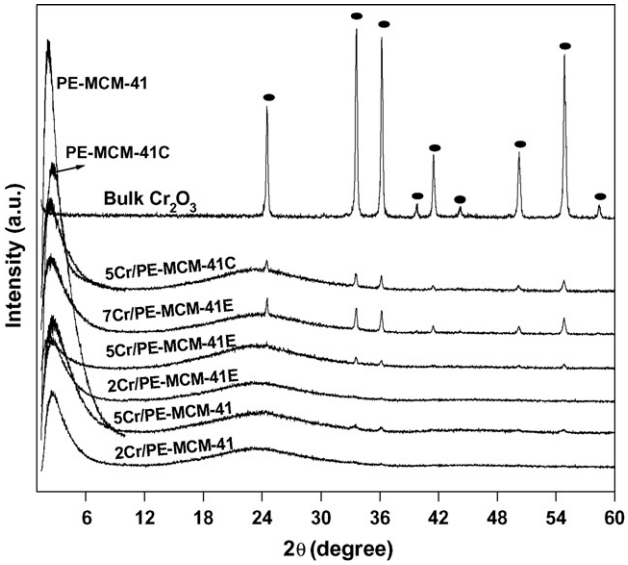


**Fig. 6.** XRD patterns of the bulk and supported chromium oxide catalysts.

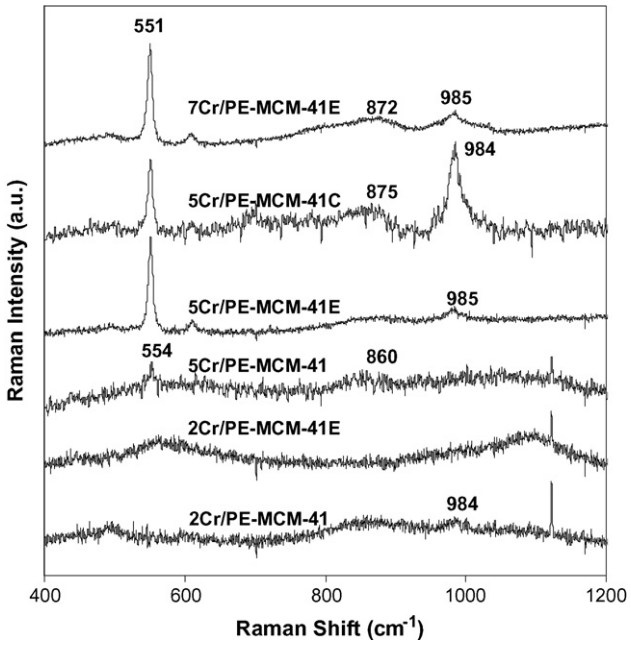


**Fig. 7.** Raman spectra for supported chromium oxide catalysts.

presence of a higher amount of crystalline $Cr_2O_3$ and/or larger $Cr_2O_3$ particles. It is also observed from Fig. 6 that when the chromia loading increases beyond 5 wt.% on PE-MCM-41E, the $Cr_2O_3$ diffraction peaks increase further, indicating additional formation of crystalline $Cr_2O_3$ with higher loading samples.

### 3.3. Raman spectroscopy

Fig. 7 reveals that all the supported chromium oxide catalysts contain both hydrated surface chromia as indicated by ~858–872 $cm^{-1}$ [34] and dehydrated surface chromia species (~985–1000 $cm^{-1}$) [34]. It is widely known that silica and silica-supported catalysts undergo extensive dehydroxylation when calcined at relatively high temperature (>550 °C). In the case of silica supported chromia, this gives rise to dehydrated surface chromium species [34,35]. It is thus inferred that the occurrence of dehydrated surface chromium species along with the hydrated species stems from the fact that all the current catalysts have been calcined at 700 °C. Nevertheless, contribution from laser-induced dehydration cannot be ruled out. As indicated by 550 $cm^{-1}$ peak in Fig. 7, Raman spectra show that $Cr_2O_3$ crystals occur in materials containing 5% Cr and higher. This is consistent with the XRD data.

### 3.4. $H_2$-TPR

The reducibility of the catalysts was investigated by $H_2$-TPR and the results are presented in Table 1 and Fig. 8. All the supported samples showed a single reduction peak at 405–415 °C, while bulk $Cr_2O_3$ showed two reduction peaks at 244 and 518 °C (broad). It appears that the temperature of maximum $H_2$ consumption ($T_{max}$) is relatively independent of chromia loading and the preparation method. Moreover, quantitative calculations shown in Table 1 indicate that hydrogen consumption (per g cat) increases with increasing chromia loading for all samples (*x*Cr/PE-MCM-41 and *x*Cr/PE-MCM-41E) prepared by different methods, and levels off at higher loadings (>5 wt.%) due to the presence of crystalline $Cr_2O_3$. As shown in Table 1 (last column), pure $Cr_2O_3$ hardly reduces. Furthermore, comparison of the ~5 wt.% chromia-containing samples revealed that the hydrogen consumption is dependent on the catalyst preparation method.

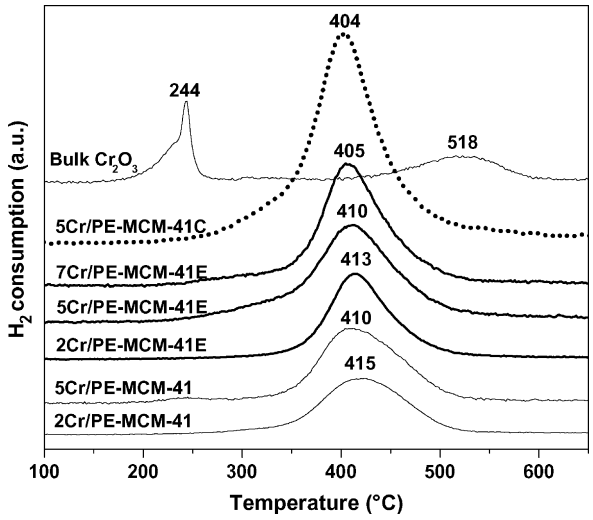


**Fig. 8.** TPR profiles of the bulk and supported chromium oxide catalysts.

Based on the hydrogen consumption for supported catalysts, the calculated H/Cr ratio was found to vary between 0.83 and 2.12 depending on the chromia loading and the preparation method. For *x*Cr/PE-MCM-41 and *x*Cr/PE-MCM-41E samples, a H/Cr value of ~2.0 was found for samples with low chromia loading (~2%), while the samples with high loadings (~5% or more) showed a value of ~1.0, suggesting that the extent of reduction in $H_2$ is lower for samples with high vs. low chromia loading, undoubtedly because of the occurrence of larger amounts of crystalline $Cr_2O_3$. However, the ~5 wt.% chromia on PE-MCM-41C showed the highest hydrogen consumption and the highest H/Cr value (2.12) among the catalysts studied. Thus, the sample prepared by Method III showed different reduction behavior in $H_2$ compared to those prepared by other methods. This finding may not be surprising because the catalyst preparation Method III led to the collapse of the pore structure and a drastic decrease in surface area, which may result in different reduction characteristics. Furthermore, the lowest hydrogen consumption and H/Cr value for bulk $Cr_2O_3$ indicates that the extent of reduction for bulk chromia is much lower compared to supported chromia. This is in line with the literature [36].

### 3.5. XPS

A typical Cr 2p XPS spectrum is shown in Fig. 9. All spectra were comprised of two main features centered ~577 and ~586.5 eV, corresponding to Cr $2p_{3/2}$ and Cr $2p_{1/2}$ photoelectrons, respectively. The spectra were deconvoluted by the peak fitting procedure to esti-

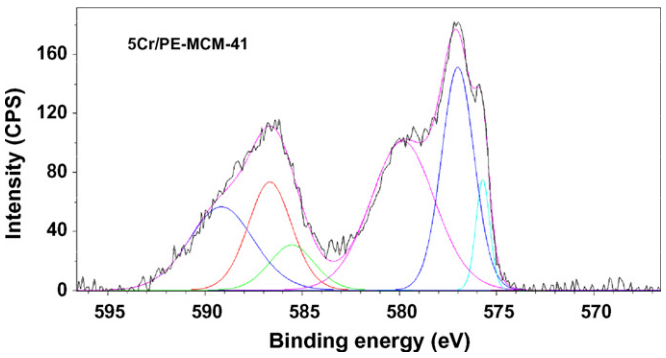


**Fig. 9.** Typical Cr 2p XPS spectrum for calcined 5%Cr/PE-MCM-41 and its deconvolution.

**Table 2**
XPS data for the supported chromium oxide catalysts.

| Catalyst | Cr $2p_{3/2}$ binding energy (eV) | | | Cr, atomic concentration (%) | Percentage of different Cr species (%) | | |
|---|---|---|---|---|---|---|---|
| | Cr(VI) | Cr(III) | Cr(II) | | Cr(VI) | Cr(III) | Cr(II) |
| 2Cr/PE-MCM-41 | – | – | – | n.d.[a] | – | – | – |
| 5Cr/PE-MCM-41 | 580.7 | 577.2 | 576.2 | 2.8 | 41.3 | 52.3 | 6.4 |
| 2Cr/PE-MCM-41E | 580.8 | 577.4 | 576.2 | 1.4 | 43.2 | 52.4 | 4.4 |
| 5Cr/PE-MCM-41E | 580.6 | 577.1 | 576.0 | 2.1 | 40.6 | 55.1 | 4.3 |
| 7Cr/PE-MCM-41E | 580.9 | 577.0 | 575.9 | 2.2 | 37.0 | 57.5 | 5.5 |
| 5Cr/PE-MCM-41C | 580.6 | 577.2 | 576.1 | 1.7 | 32.1 | 37.5 | 30.4 |

[a] n.d.: not determined.

mate the composition of chromium species stabilized in different oxidation states. This procedure revealed three different chemical states of chromium with Cr $2p_{3/2}$ binding energy values of ~576, ~577 and ~581 eV, which correspond to Cr(II), Cr(III) and Cr(VI) species, respectively [28,37]. The XPS-derived relative concentrations of the different chromium species are summarized in Table 2. The data for ~5 wt.% chromia-loaded samples (Table 2) indicate that the speciation of chromium is strongly dependent on the preparation method. Indeed, Method III resulted in a different composition of surface chromium species compared to that for Methods I and II, which led to a relatively similar surface composition of chromium species. This may be related to the different pore structure of the catalyst prepared by Method III and to the extent of chromium oxide crystallization.

XPS surveys also allowed the determination of the chromium overall surface concentration (Table 2). Again, it appears that the Cr surface concentration depends on the preparation method. For xCr/PE-MCM-41E catalysts, the atomic surface concentration of Cr increased with increasing chromia loading up to 5 wt.% and then reached a plateau at higher loadings.

## 4. Conclusions

Supported chromium oxide materials were prepared using as-synthesized, solvent extracted and calcined pore-expanded silica as support. Nitrogen adsorption measurements revealed that the average pore size and PSD depend on the nature of the starting mesophase used as support. Materials prepared using PE-MCM-41 whose pore walls were protected against water attack by the occulded surfactant (CTMA) and expander (DMDA) exhibited the most open pore structure. The XPS analysis showed that three types of Cr species, namely Cr(II), Cr(III) and Cr(VI) were present on the fresh catalysts and the speciation of surface Cr species depended on the preparation method. These properties will be correlated with the ethane dehydrogenation ability of the catalysts in a separate report [17].

## Acknowledgements

A.S. thank the Canadian Government for a Canada Research Chair in *Nanostructured Materials for Catalysis and Separation* (2001–2015). The generous support of the Natural Sciences and Engineering Research Council of Canada (NSERC) is acknowledged. Thanks to Mr. M.R. Pynenburg and Mr. R. Serna-Guerrero for their assistance with the synthesis of large-pore MCM-41 material and the TGA experiments, respectively.

## References

[1] B.M. Weckhuysen, R.A. Schoonheydt, Catal. Today 51 (1999) 223.
[2] M.M. Bhasin, J.H. McCain, B.V. Vora, T. Imai, P.R. Pujado, Appl. Catal. A: Gen. 221 (2001) 397.
[3] D. Sanfilippo, I. Miracca, Catal. Today 111 (2006) 133.
[4] F.M. Ashmawy, J. Chem. Soc. Faraday Trans. I 76 (1980) 2096.
[5] H.J. Lugo, J.H. Lunsford, J. Catal. 91 (1985) 155.
[6] H. Yang, L. Xu, D. Ji, Q. Wang, L. Lin, React. Kinet. Catal. Lett. 76 (2002) 151.
[7] A. Tsyganok, P.J.E. Harlick, A. Sayari, Catal. Commun. 8 (2007) 850.
[8] A. Tsyganok, R.G. Green, J.B. Giorgi, A. Sayari, Catal. Commun. 8 (2007) 2185.
[9] U. Olsbye, A. Virnovskaia, O. Prytz, S.J. Tinnemans, B.M. Weckhuysen, Catal. Lett. 103 (2005) 143.
[10] B.M. Weckhuysen, A. Bensalem, R.A. Schoonheydt, J. Chem. Soc. Faraday Trans. 94 (1998) 2011.
[11] S. De Rossi, G. Ferraris, S. Fremiotti, E. Garrone, G. Ghiotti, M.C. Campa, V. Indovina, J. Catal. 148 (1994) 36.
[12] F. Cavani, M. Koutyrev, F. Trifiro, A. Bartolini, D. Ghisletti, R. Iezzi, A. Santucci, G.D. Piero, J. Catal. 158 (1996) 236.
[13] Y. Ohishi, T. Kawabata, T. Shishido, K. Takaki, Q. Zhang, Y. Wang, K. Takehira, J. Mol. Catal. A: Chem. 230 (2005) 49.
[14] K. Takehira, Y. Ohishi, T. Shishido, T. Kawabata, K. Takaki, Q. Zhang, Y. Wang, J. Catal. 224 (2004) 404.
[15] A. Jiménez-López, E. Rodríguez-Castellón, P. Maireles-Torres, L. Díaz, J. Mérida-Robles, Appl. Catal. A: Gen. 218 (2001) 295.
[16] B.M. Weckhuysen, R.R. Rao, J. Pelgrims, R.A. Schoonheydt, P. Bodart, G. Debras, O. Collart, P.V.D. Voort, E.F. Vansant, Chem. Eur. J. 6 (2000) 2960.
[17] T.V.M. Rao, E. Zahidi, A. Sayari, J. Mol. Catal. A: Chem 301 (2009) 159.
[18] A. Sayari, M. Kruk, M. Jaroniec, I.L. Moudrakovski, Adv. Mater. 10 (1998) 1376.
[19] A. Sayari, Angew. Chem. Int. Ed. 39 (2000) 2920.
[20] M. Kruk, M. Jaroniec, V. Antochshuk, A. Sayari, J. Phys. Chem. B 106 (2002) 10096.
[21] P.J.E. Harlick, A. Sayari, Ind. Eng. Chem. Res. 45 (2006) 3248.
[22] R. Serna-Guerrero, A. Sayari, Environ. Sci. Technol. 41 (2007) 4761.
[23] K.-Z. Hossain, C.M. Monreal, A. Sayari, Colloid. Surf. B: Biointerf. 62 (2008) 42.
[24] D.D. Das, P.J.E. Harlick, A. Sayari, Catal. Commun. 8 (2007) 829.
[25] M. Kruk, M. Jaroniec, A. Sayari, Langmuir 13 (1997) 6267.
[26] I. Martyanov, A. Sayari, Catal. Lett. 126 (2008) 164.
[27] R. Merryfield, M. McDaniel, G. Parks, J. Catal. 77 (1982) 348.
[28] B. Liu, Y. Fang, M. Terano, J. Mol. Catal. A: Chem. 219 (2004) 165.
[29] A.B. Gaspar, C.A.C. Perez, L.C. Dieguez, Appl. Surf. Sci. 252 (2005) 939.
[30] A. Sayari, Y. Yang, M. Kruk, M. Jaroniec, J. Phys. Chem. B 103 (1999) 3651.
[31] A. Sayari, P. Liu, M. Kruk, M. Jaroniec, Chem. Mater. 9 (1997) 2499.
[32] M. Kruk, M. Jaroniec, A. Sayari, Micropor. Mesopor. Mater. 35–36 (2000) 545.
[33] K.A. Koyano, T. Tatsumi, Y. Tanaka, S. Nakata, J. Phys. Chem. B 101 (1997) 9436.
[34] F.D. Hardcastle, I.E. Wachs, J. Mol. Catal. 46 (1988) 173.
[35] M.P. McDaniel, J. Catal. 67 (1981) 71.
[36] B. Grzybowska, J. Sloczynski, R. Grabowski, K. Wcislo, A. Kozlowska, J. Stoch, J. Zielinski, J. Catal. 178 (1998) 687.
[37] B.M. Weckhuysen, I.E. Wachs, R.A. Schoonheydt, Chem. Rev. 96 (1996) 3327.